



Form drag in rivers due to small-scale natural topographic features: 2. Irregular sequences

Jason W. Kean¹ and J. Dungan Smith¹

Received 20 February 2006; revised 5 July 2006; accepted 14 August 2006; published 6 December 2006.

[1] The size, shape, and spacing of small-scale topographic features found on the boundaries of natural streams, rivers, and floodplains can be quite variable. Consequently, a procedure for determining the form drag on irregular sequences of different-sized topographic features is essential for calculating near-boundary flows and sediment transport. A method for carrying out such calculations is developed in this paper. This method builds on the work of Kean and Smith (2006), which describes the flow field for the simpler case of a regular sequence of identical topographic features. Both approaches model topographic features as two-dimensional elements with Gaussian-shaped cross sections defined in terms of three parameters. Field measurements of bank topography are used to show that (1) the magnitude of these shape parameters can vary greatly between adjacent topographic features and (2) the variability of these shape parameters follows a lognormal distribution. Simulations using an irregular set of topographic roughness elements show that the drag on an individual element is primarily controlled by the size and shape of the feature immediately upstream and that the spatial average of the boundary shear stress over a large set of randomly ordered elements is relatively insensitive to the sequence of the elements. In addition, a method to transform the topography of irregular surfaces into an equivalently rough surface of regularly spaced, identical topographic elements also is given. The methods described in this paper can be used to improve predictions of flow resistance in rivers as well as quantify bank roughness.

Citation: Kean, J. W., and J. D. Smith (2006), Form drag in rivers due to small-scale natural topographic features: 2. Irregular sequences, *J. Geophys. Res.*, *111*, F04010, doi:10.1029/2006JF000490.

1. Introduction

[2] In our companion paper [Kean and Smith, 2006], we describe a simple method to quantify the flow effects of regular sequences of small-scale natural topographic features characteristic of stream banks. There it is shown that a wide variety of natural bank topographic features can be well approximated by shapes with Gaussian cross sections. This shape is parameterized in terms of a protrusion height, H ; a streamwise length scale, σ , (equivalent to the standard deviation of a Gaussian probability distribution); and a spacing between crests, λ . The method of Kean and Smith [2006] uses an approach similar to that of Smith and McLean [1977] for flow over dunes to describe the spatially averaged flow over a sequence of identical Gaussian-shaped topographic elements. The measurements of Hopson [1999] were used to demonstrate that the form drag on a roughness element embedded in a series of identical elements can be determined using the drag coefficient of the individual element and a reference velocity that includes the effects of roughness elements further upstream.

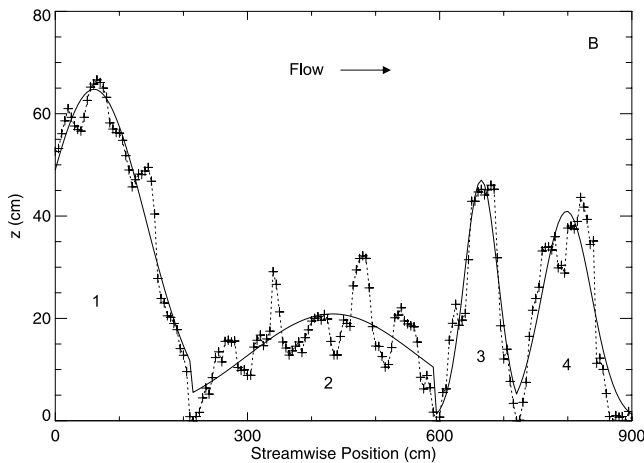
[3] While the method of Kean and Smith [2006] addresses many of the salient aspects of flow over natural

surfaces, it does not address the flow effects of surface irregularity. Natural topography is almost always irregular, and often the surface roughness and irregularity is most pronounced along the banks of the channel. Common irregularities in bank topography include undulations produced by the slumping of bank material and protrusions associated with vegetation, such as root balls and clumps of grass sod. A wide variety of factors, such as flow, soil cohesion, and vegetation, influence the geometry of these bank topographic features. As a result, there is considerable variability in the size and shape of nearby topographic features. The form drag produced by flow over this spectrum of different sized roughness elements can have a significant effect on the velocity and boundary shear stress. These effects are especially important near the banks of channels, because they control the rates of sediment transport at the base of the bank, which, in turn, controls the rate of lateral erosion. Quantifying the roughness of natural surfaces, however, is particularly difficult due to its complexity. For this reason, the roughness of irregular surfaces is frequently parameterized in terms of an empirically adjusted roughness coefficient. Limitations of this empirical approach are that it requires calibration, that the roughness of the surface cannot be easily tied to the geometry of the surface, and that the form drag on the topographic elements of the surface cannot be removed to obtain the shear stress

¹U.S. Geological Survey, Boulder, Colorado, USA.



a.



b.

Figure 1. Characterization of the small-scale bank roughness. (a) Bank of the inset channel of the Rio Puerco near Belen, New Mexico. A 9-m straight edge is used as a reference for measurements of the amplitude of the topographic elements at 5-cm intervals. The amplitude of the elements increases from bottom to top of the bank. (b) Measurements and Gaussian fit of the topographic elements near the top of the bank and bump numbers (Table 1).

on the actual (irregular) surface as required to carry out accurate sediment transport and erosion calculations.

[4] The purpose of this paper is to generalize the method of *Kean and Smith* [2006] to accommodate the irregular sequences of topographic elements characteristic of natural streams and rivers. The general model is then applied to assess the relative importance of size, shape, and sequence of topographic elements on a boundary using elements that are modeled after ones on the banks of the Rio Puerco near Belen, NM. A method to simplify the topography of irregular surfaces into an equivalently rough surface of regularly spaced, identical topographic elements also is presented. The results of that analysis are then used to provide a generalized model for the geometry of a boundary in terms of the geometrical statistics of an irregular surface.

[5] The approach of *Kean and Smith* [2006] and of this paper is to first identify distinct topographic features along an irregular surface, then approximate each feature as a two-dimensional Gaussian-shaped element, and finally calculate the form drag on each of the individual elements. Drag is a nonlinear process governed by the Navier-Stokes or Reynolds equations. Owing to this nonlinearity the ways in which form drag can be computed are tightly constrained. Moreover, form drag is an integral fluid mechanical variable and must be computed on entire objects or large segments thereof. Both the nonlinearity of the drag process and the integral nature of form drag make it impossible to compute drag on and sum the contributions of drag from individual harmonic components.

[6] Drag arises from the pressure field generated around an object inserted into a flow. As such, it requires that there be a protrusion from a background surface when applied to the topographic elements on a flow boundary. The background surface cannot be the mean surface. We employ a low wave number background surface constructed by connecting the troughs of the topographic elements. If, as in the next section, a Fourier analysis of the topographic variability is employed, it has to have a distinct spectral peak and all of the topographic variance has to be placed in a single sinusoid before the drag on that surface can be calculated. In addition, the surface around which the sinusoid oscillates cannot be used as the background surface; rather the form drag on the sinusoidal topography has to be calculated from a smooth surface that goes through all the troughs of the sinusoid.

2. Variability of Natural Topographic Features

2.1. Rio Puerco, New Mexico

[7] An example of the variability of natural surfaces can be seen from the streamwise profile of bank topography measured in the inset channel of the Rio Puerco arroyo near Belen, New Mexico (Figure 1). These measurements were made as part of a larger study of the Rio Puerco, and will be used here to (1) demonstrate that Gaussian curves provide good approximations to the shape of natural topographic elements [see also *Kean and Smith*, 2005, 2006], and (2) provide a realistic scale for topographic elements that will be used in later calculations in this paper.

[8] The roughness of the Rio Puerco banks at Belen is produced by both the topographic irregularities resulting from scour and mass movement of bank material and from the tamarisk trees, which, as shown in Figure 1a, have been removed so that the geometry of the irregularities beneath could be measured. The effect of the vegetation on the flow in this channel is discussed by *Kean and Smith* [2004] and *Griffin et al.* [2005]. The roughness measurements were made by placing a 9-m straight edge along the bank and determining the distance from the straight edge to the bank at 5-cm intervals. This approach provided a good sample of the amplitude and spacing of the topographic irregularities. The set of measurements shown in Figure 1b contain four large, roughly symmetric bumps (topographic features) that are spaced close together: a tall bump, a broad bump, a steep bump, and an intermediate bump, which will each have a different effect on the flow. A best fit Gaussian shape for each bump was determined by regression, and the results

Table 1. Gaussian Fit for Measured Rio Puerco Bumps

Bump	H , m	σ , m	σ/H	C_D	$C_D H$, m
1	0.63	0.85	1.35	0.63	0.40
2	0.23	1.14	4.96	0.04	0.01
3	0.49	0.29	0.59	1.13	0.55
4	0.40	0.41	1.03	0.81	0.32
Deviations	0.15	0.14	0.93	0.87	0.14

are listed in Table 1. As is seen in Figure 1b, the Gaussian shapes provide good approximations to the variations of the surface. Table 1 also contains an estimate of the drag coefficient (C_D) for each bump determined using the expression by *Kean and Smith* [2006], which is

$$C_D = 1.79 \exp\left(-0.77 \frac{\sigma}{H}\right) \quad (1)$$

where σ is the streamwise length scale for the element, and H is the protrusion height of the element. For the flows of interest in this study ($Fr < 1$, $1 \times 10^3 < Re < 5 \times 10^5$) C_D is nearly independent of the Reynolds and Froude numbers.

[9] The product of the element's drag coefficient and height provides some indication of the relative effects these bumps will have on the flow. This product scales the drag on the element, as well as the velocity deficit of its wake, which, in turn, affects the drag on elements located downstream. Using this simple measure, it appears that the steepest bump (bump 3) will have the highest drag and the greatest effect on reducing the drag on the elements downstream. In addition, it also will transmit considerable stress to the boundary, because of its short span. Conversely, the product $C_D H$ shows that the large-scale shape of bump 2 can be neglected in favor of determining the drag on the smaller-scale features covering this bump.

[10] The geometric characteristics of these smaller-scale features were determined from a Fourier analysis of the deviations from the Gaussian fit of the four bumps. The deviations and their power spectrum are shown in Figure 2. The well-defined peak in the power spectrum shows that these features have a single characteristic spacing corresponding to about 70 cm, and can be approximated by a single sine wave with this wavelength. In order to preserve the variance of the features, the amplitude, H , of this sine wave was set such that the average squared height of the sine wave over one wavelength, $(1/\lambda) \int_0^\lambda [H \sin(2\pi x/\lambda)]^2 dx$, was equal to the variance of the measured deviations. Although the sine wave provides a good approximation to the typical shape of the small-scale features, it does not provide a measure of the flow resistance of these features, because the drag coefficient of a sine-shaped bump is not known. For this reason, the sine wave was approximated by a sequence of Gaussian bumps determined by regression. The fit parameters and estimated drag coefficient for these bumps are listed in Table 1. As seen in Figure 2c, the sequence of Gaussian bumps is a good approximation to the sine wave.

[11] It should be noted here that while Fourier analysis was used to identify the size of the small-scale features, form drag could not be calculated on each of the individual harmonics and then summed. Instead, all of the variance had to be placed into a single sinusoid, the reference surface had to be transformed to the troughs of the sinusoid, and the

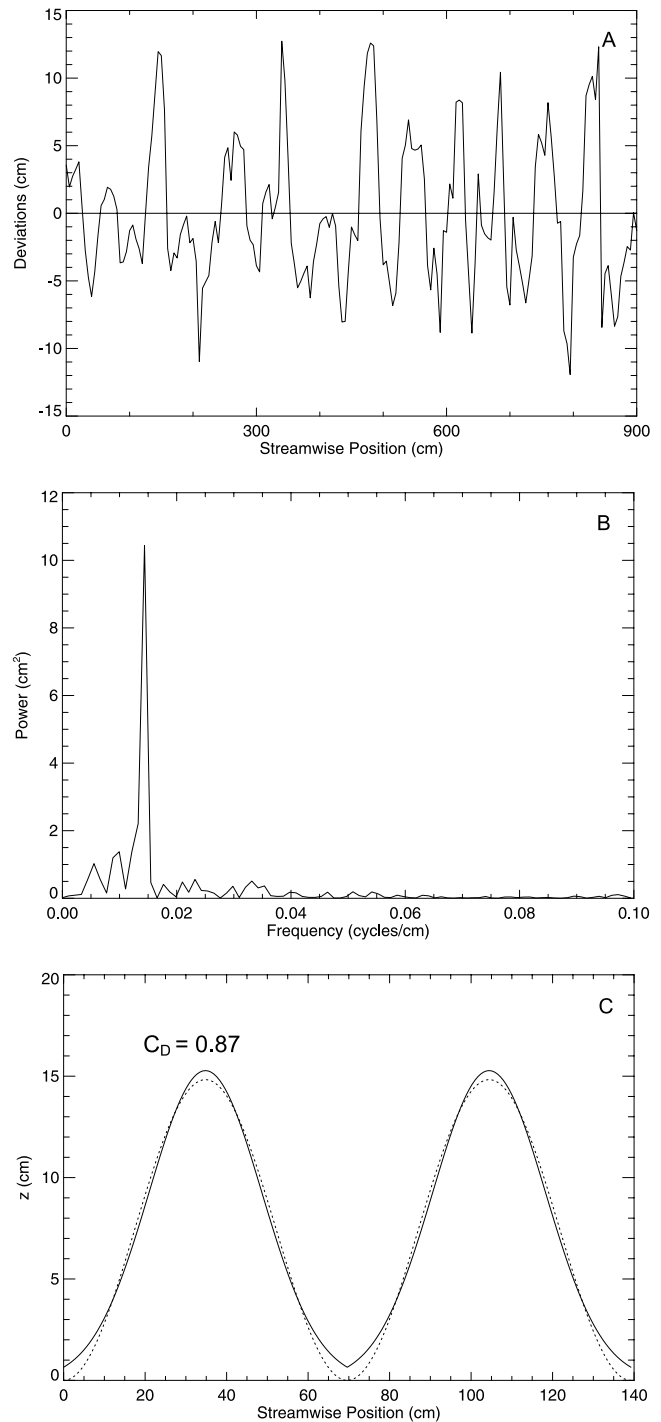


Figure 2. Characterization of the finer scale of bank roughness. (a) Deviations from the fit of the topographic elements shown in Figure 1b (note the change in the vertical scale between Figures 1 and 2). (b) Power spectrum of the deviations. The peak in the spectrum corresponds to a wavelength of 70 cm. (c) Approximation of the deviations using a sine wave (dotted line) and Gaussian curves (solid line). The wavelength of the sine curve is 70 cm.

sinusoidal features had to be approximated as Gaussian ones. This is because Fourier analysis cannot be used in conjunction with nonlinear operators such as form drag.

[12] The well-defined peak in the power spectrum suggests that the geometry of the smaller scale of roughness is shaped by an underlying physical process. This process is probably related to deposition of fine-grained sediment on the banks of the Rio Puerco, which has been documented by *Friedman et al.* [2005]. Floods in the Rio Puerco typically have very high suspended sediment concentrations. The reduced flow velocities near the bank caused by drag on the vegetation and topographic features, leads to rapid deposition of the suspended sediment on the banks. The bank angles cannot support the continual supply of sediment, and the excess is transported down the bank by mass movement. It is likely that this continual sloughing process sets the geometry of the small-scale roughness. This process also affects the shape of the large-scale features, but their geometry is complicated by the trunks of the tamarisk trees, which retard the sloughing. Calculations of drag on roughness elements having a similar geometry as that of the small-scale roughness on the banks of the Rio Puerco near Belen will be presented later in this paper.

2.2. Statistical Properties

[13] Additional insight into the variability of natural bank surfaces can be obtained by analyzing the statistical properties of the surface topography. This is done here using three sets of bank roughness measurements that were made near U.S. Geological Survey (USGS) streamflow gauging stations. The stations are 12323840, Lost Creek near Anaconda, MT; 07146995, Rock Creek near Potwin, KS; and 07147070, Whitewater River at Towanda, KS. These sites span a wide range in channel size and have banks composed of different materials and shaped by different mechanisms. Despite these differences, the topographic features at these sites, like the Rio Puerco, are well approximated by shapes with Gaussian cross sections [see *Kean and Smith*, 2006]. In addition to having bank features that are Gaussian in shape, the bank topography at the sites also has several important statistical properties in common, as will be discussed below.

[14] Figure 3 shows histograms of the size distributions of H , σ , and λ at each of the sites. The parameters were obtained from the best fit Gaussian curve to each topographic feature identified in the measurements. For irregular sequences of features such as these, λ for an individual feature is defined to be the distance between the intersections of its Gaussian curve with the Gaussian curves of the upstream and downstream features. The sizes of each of the parameters are binned in equal logarithmic increments. As seen in Figure 3, the average size of the sampled topographic features at each of the sites varies considerably. For example, the median σ varies from 5.2 cm at Lost Creek to 82 cm at Whitewater River. Note that the breadth scale is 2σ . Variations in the average geometry of the features at the sites are due to differences in both the size of the channel and the environmental factors that control the shape of the features.

[15] A chi-square goodness of fit test was performed on all of the parameters to test the hypothesis that they are lognormally distributed. The probability (P) of obtaining a chi-square value greater than the value computed for each

distribution is shown in Figure 3 for each parameter. Greater values of P mean the data more closely fit the assumed distribution. If P is greater than 0.10, the hypothesis that the distribution is lognormal cannot be rejected at the 10% significance level. On the basis of this statistical test, the size distributions of H , σ , and λ at all of the sites can be considered lognormal.

[16] Additional histograms of important combinations of H , σ , and λ are shown in Figure 4. These combinations are: σ/H , the primary measure of the shape of the feature; λ/σ , the ratio of the two streamwise length scales; and the product, $C_D H$, a measure of the intensity of the wake produced by flow past the feature. Many, but not all, of these variables can be considered lognormally distributed based on the statistical test described above. Like the primary geometric parameters (H , σ , and λ), these parameters also vary considerably between sites. For example, the median shape, $(\sigma/H)_{50}$, of the features varies from “sharp” (0.9 at Lost Creek) to “broad” (4.6 at Whitewater River).

[17] In addition to having similar statistical distributions, there are several other important similarities between the statistics of the bank features at the sites. Some of these similarities can be seen from Table 2, which lists the mean (μ) and standard deviation (v) of the natural logarithm of H , σ , and λ . Despite substantial differences in the means for each variable, the standard deviation of each parameter falls within a fairly narrow range. The same is true for the standard deviations of the logarithms of the ratios σ/H , λ/σ , and λ/H , which are given in Table 3 together with the correlation between the two variables defining each ratio. Table 3 shows that the two streamwise length scales σ and λ are strongly correlated at all sites. The sites also have comparable, but weaker, $\sigma-H$ and $\lambda-H$ correlations.

3. Model Development for an Irregular Sequence of Topographic Features

[18] The flow over an irregular sequence of topographic features, such as the one shown in Figure 1b, is similar to the flow over a regular sequence of elements, which is described in the companion paper [*Kean and Smith*, 2006]. In both cases, determination of the flow field over the sequence requires calculating the form drag on the individual elements. For irregular sequences, this calculation is complicated by the fact that the form drag on each element is unique as a result of its size, shape, and location relative to the other elements in the array. This section (1) provides a brief overview of the model for the regular sequence and its relation to the present model, (2) outlines important distinctions in the definition of certain variables between the two models, and (3) describes the additional model components that are required to generalize the method of *Kean and Smith* [2006] to include the effects of topographic variability on the flow field. The reader is referred to the companion paper for a description of equations that form the core of the model for the irregular sequence.

[19] The drag (F) on an individual element is given by the equation

$$F = \frac{1}{2} \rho C_D H B u_{ref}^2 \quad (2)$$

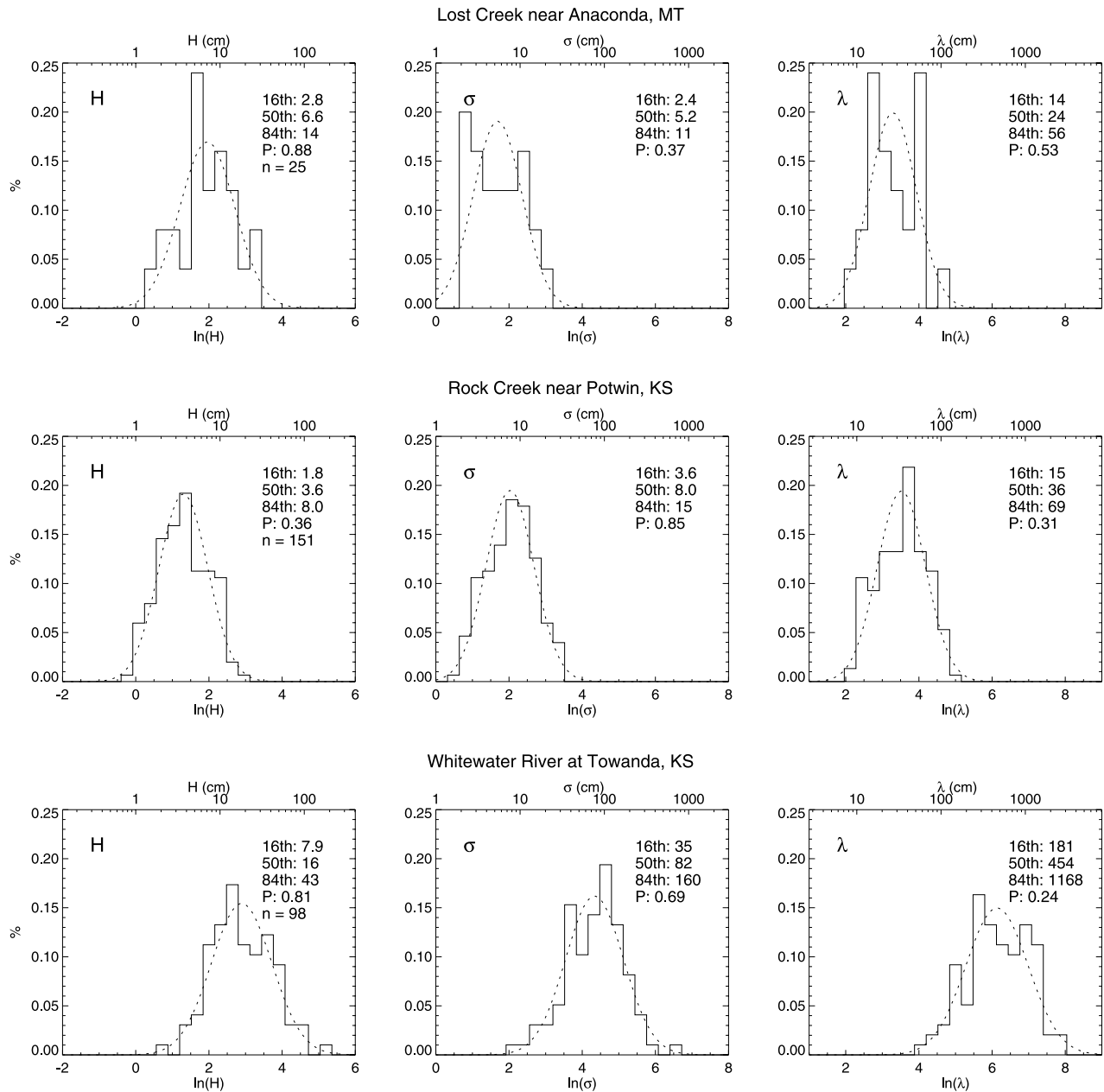


Figure 3. Histograms of H , σ , and λ (in units of centimeters) for measured bank topographic features near three USGS streamflow gauging stations. The number (n) of topographic features in each sample is listed for each site. A continuous lognormal distribution defined by the mean (μ) and standard deviation (ν) of the natural logarithm for each variable is shown for comparison (dotted line). A statistical measure (P) of how well the data follow a lognormal distribution also is given for each variable. For reference, the approximate bankfull discharges for Lost Creek, Rock Creek, and Whitewater River are 5, 20, and 150 m^3/s , respectively.

where ρ is the density of water, B is the length of the element in the direction perpendicular to the x and z axis, and u_{ref} is an appropriately determined reference velocity. The square of the reference velocity is defined to be the average of the square of the velocity that would be present if the element were removed from the flow. A robust estimate of u_{ref} can be made by averaging the square of the velocity over the volume the element occupies (see Figure 2 of *Kean and Smith* [2006]). The velocity in this area primarily is

affected by three interdependent regions each having turbulent processes which scale differently. They are an internal boundary layer region, a wake region, and an outer boundary layer region. The model of *Kean and Smith* [2006] describes the velocity in each region separately and joins them together using appropriate matching conditions. The three interdependent regions also are present in flows over irregular sequences of topographic elements and can be described using same equations with relatively minor

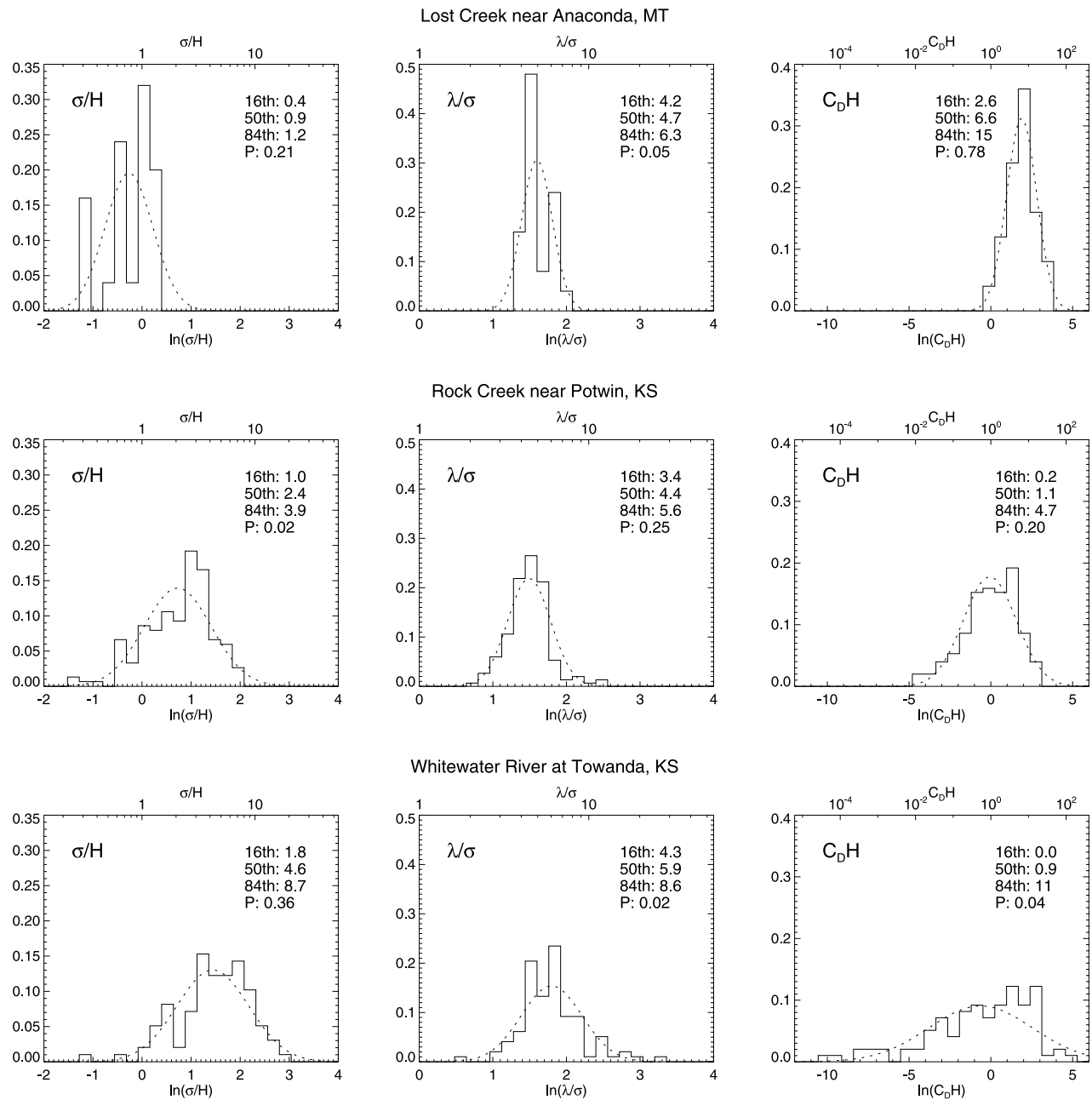


Figure 4. Histograms of σ/H , λ/σ , and $C_D H$ for the same measured bank topographic features shown in Figure 3. The percentiles for $C_D H$ are given in units of centimeters. A continuous lognormal distribution defined by μ and ν for each variable is shown for comparison (dotted line).

modification that will be outlined later. For irregular sequences, the reference velocity is particularly sensitive to the relative location of the element within the array. For example, the reference velocity (and drag) on a small bump downstream from a large one is relatively low, because it is well inside the wake of the large bump upstream. Conversely, the reference velocity on a large bump downstream from a small one is hardly affected by the wake of the small bump upstream, because much of the large bump is above the wake of the small bump. In both cases, the reference velocity also depends on the geometry of the bumps further upstream. The momentum deficit produced by drag on these upstream bumps causes momentum to diffuse in toward the boundary

and creates an evolving outer velocity profile, which, in turn, scales the wake of each bump. Thus the flow and boundary shear stress over an irregular boundary depend on a complicated interaction of the various elements.

Table 2. Statistics of Geometric Parameters of Measured Bank Topographic Features

Site	n	H		σ		λ	
		μ	ν	μ	ν	μ	ν
Lost C.	25	1.96	0.74	1.69	0.66	3.29	0.63
Rock C.	151	1.30	0.67	2.03	0.66	3.52	0.66
Whitewater R.	98	2.89	0.83	4.34	0.79	6.13	0.85

Table 3. Statistics of Combinations of Geometric Parameters of Bank Topographic Features

Site	σ/H			$\lambda\sigma$			λ/H		
	μ	ν	Correlation	μ	ν	Correlation	μ	ν	Correlation
Lost C.	-0.27	0.48	0.66	1.60	0.21	0.97	1.33	0.53	0.71
Rock C.	0.73	0.69	0.51	1.49	0.29	0.93	2.22	0.60	0.60
Whitewater R.	1.44	0.73	0.69	1.80	0.42	0.87	3.24	0.67	0.75

[20] Several important distinctions in the meaning of some of the variables defined by *Kean and Smith* [2006] must be made in order to generalize the equations to apply to the case of an irregular sequence. First, as mentioned earlier, λ for an individual element in an irregular sequence is not always equivalent to the spacing between crests as it was in the regular model. Rather, for the irregular problem, λ for an individual feature is the distance between the intersections of its Gaussian curve with the Gaussian curves of the upstream and downstream features. The second important distinction concerns the application of the empirical equation for β (equation (17) of *Kean and Smith* [2006]), which is a constant that sets the eddy viscosity in the wake. In the *Kean and Smith* [2006] formulation, the value of β is adjusted empirically as a function of λ and H . This adjustment accounts for near-field flow effects that are present for closely spaced sequences, which are not accounted for in the far-field wake solution employed by the model [*Schlichting*, 1979]. Unlike the regular case addressed in the companion paper, H and λ vary for each element in an irregular sequence. In this situation, a value of β must be defined for each element in the sequence. For a given element, the appropriate value of H to be used in the equation for β is the H for the upstream object producing the wake, and the corresponding value for λ is the distance between the crests of the two elements.

3.1. Change in Uniform Roughness

[21] Before treating flow over an irregular sequence, it is useful to first examine the simpler case of an abrupt change in surface roughness from one uniform set of elements to another set having a different roughness height due to skin friction plus form drag (z_{oT}). This problem has received considerable attention in the atmospheric literature, with regard to the change of a wind profile from one surface condition to another, such as from a field to a forest or vice versa. Diagrams of smooth-to-rough and rough-to-smooth changes in uniform sets of roughness elements are shown in the background of Figure 5. As a flow, which is in equilibrium with the surface beneath it, encounters a rougher surface, it decelerates as a consequence of the greater resistance of the new surface. The opposite occurs in a transition to a smoother surface, where the flow accelerates because the new surface offers less resistance. These effects are initially felt only very near the boundary, but diffuse upward to form a new growing boundary layer. The flow in this layer evolves to be in equilibrium with the new boundary. The thickness of this new layer can be described using the same formulation that was used to describe the growth of the internal boundary layer downstream from the separation zone behind a roughness element [*Miyake*, 1965]. In order to distinguish between the two types of internal boundary layers, the higher internal boundary layer, associated with the change in roughness, will

be referred to as a disturbance layer. The equation for the thickness of the disturbance layer (δ_{DL}) is given by

$$\frac{\delta_{DL}}{x''} \left[\ln \left(\frac{\delta_{DL}}{z_{oT}} \right) - 1 \right] = \gamma \kappa \quad (3)$$

where x'' is the distance downstream from the beginning of the disturbance layer, z_{oT} is the total roughness height of the downstream surface, κ is von Karman's constant = 0.408 [*Long et al.*, 1993], and γ is a constant = 1.25 [*Walmsley*, 1989].

[22] Above the disturbance layer, the flow is unaffected by the roughness change and thus has the same structure it

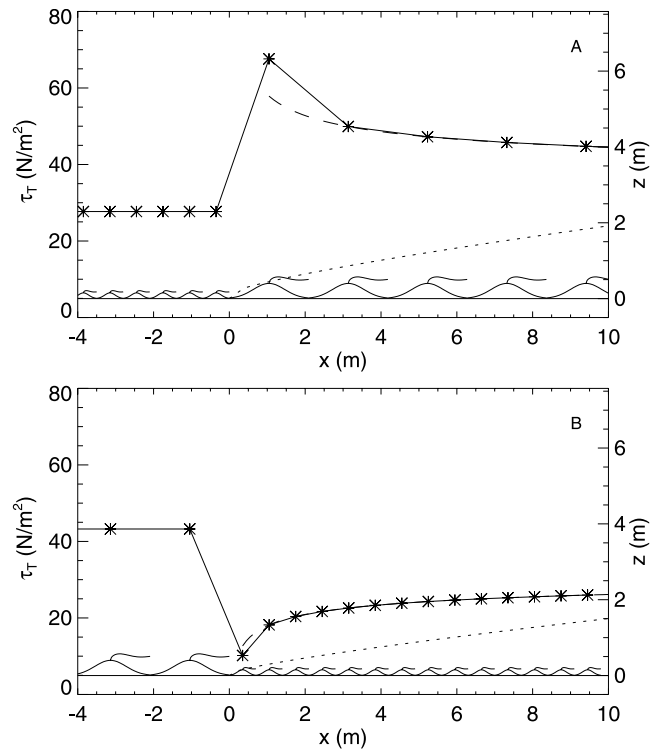


Figure 5. Calculations of the total boundary shear stress averaged over each bump (symbols) for (a) smooth-to-rough transition and (b) rough-to-smooth transition. The boundary shear stress calculated using (4) is shown with the dashed line and gives the same result for all but the first element in the change in roughness. The geometry of the elements is drawn in the background together with the top of the first part of the wake for each element and the growth of the disturbance layer (dotted line). The shear velocity of the upstream flow is 0.17 m/s for Figure 5a and 0.21 m/s for Figure 5b. In both cases the upstream velocity at $z = 2.5$ m is 2 m/s.

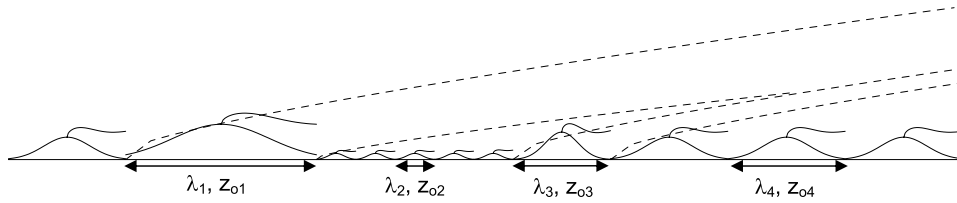


Figure 6. Diagram of multiple disturbance layers (dashed line) produced by different types of roughness elements. The faster growing disturbance layer produced by the z_{o3} element envelopes the slower growing layer of the smaller z_{o2} elements. The top of the first part of the wake for each element is also shown (solid line). Element types 1–4 are as in Table 4.

did upstream from the change in bed roughness. Within the disturbance layer, the flow develops a structure associated with the new roughness. As a result, there is a distinct slope change in the velocity profile at the interface between the two regions. *Elliot* [1958] assumed that the velocity profile within the disturbance layer was logarithmic and characterized by the roughness height of the new surface. Equating the upstream and downstream logarithmic profiles at the height of the disturbance layer gives an expression for the boundary shear stress as a function of position downstream (x) from the roughness change

$$\frac{\tau_{T2}(x)}{\tau_{T1}} = \left[1 - \frac{\ln(z_{oT1}/z_{oT2})}{\ln(\delta_{DL}(x)/z_{oT2})} \right]^2 \quad (4)$$

where τ_{T1} and z_{oT1} are the total boundary shear stress and total roughness height of the upstream surface, and τ_{T2} and z_{oT2} are the same parameters for the downstream surface. This simple assumption has been shown to be in good agreement with atmospheric measurements [*Kaimal and Finnigan*, 1994].

[23] Assuming the flow near the top of the disturbance layer has developed a logarithmic structure, the form drag on all but the first bump downstream from the roughness change can be determined using the form drag model for regular sequence of elements [*Kean and Smith*, 2006], and the velocity at the top of the disturbance layer, which can be determined from the upstream profile. For the first bump of the roughness change, it is assumed the disturbance layer does not affect the drag, because the flow within the disturbance layer has not had sufficient time to organize into a logarithmic profile. The drag on this bump is produced primarily from the upstream flow, and can be calculated using the drag equation (2) and a reference velocity determined from the upstream flow. Specifically, the reference velocity is calculated by averaging the upstream profile over the area of the first bump through the equation

$$u_{ref}^2 = \frac{1}{A} \int_A u^2(x, y) dA \quad (5)$$

where A is the plan view area of the element. The plan view area of a Gaussian shape is given by $H\sigma\sqrt{\pi/2} \left[\text{erf}\left(\frac{x_{dn}-x_c}{\sqrt{2}\sigma}\right) - \text{erf}\left(\frac{x_{up}-x_c}{\sqrt{2}\sigma}\right) \right]$, where x_{up} , x_{dn} , and x_c are the streamwise positions of the upstream end, downstream end, and center (crest) of the element, respectively. As in the case of the regular sequence, the upstream profile

in this case consists of three flow regions matched together in the same manner. They are (1) the outer logarithmic region of the upstream sequence, and (2) the wake and (3) the internal boundary layer of the last bump of the upstream sequence. Depending on the protrusion height of the element, the integral for the u_{ref} may include only the lowest region, the lowest two regions, or all three regions.

[24] These methods were used to determine the boundary shear stress for a hypothetical flow over the two boundaries shown in the background of Figure 5. The flow is modeled as very deep, and consequently, there is no significant change in the free surface elevation due to the roughness differences. The roughness elements for the two surfaces were modeled after the Rio Puerco measurements. The smoother surface was modeled after the deviation bumps with $\lambda = 0.70$ m and the rough surface was modeled after the fourth bump with $\lambda = 2.09$ m. The skin friction roughness height, z_{oSF} , used for both surfaces is 1.0×10^{-4} m. The roughness heights for these two surfaces were determined to be $(z_{oT})_{smooth} = 1.9 \times 10^{-2}$ m and $(z_{oT})_{rough} = 4.9 \times 10^{-2}$ m using the method of *Kean and Smith* [2006]. Figure 5 shows the total boundary shear stress averaged over each unit “cell” for both a smooth-to-rough change and a rough-to-smooth change. The “cell” is the region, of length λ , between the end of the upstream element and the beginning of the downstream element as shown in Figure 6. The total boundary shear stress calculated using (4) also is shown for comparison in Figure 5. With the exception of the first bump, the two methods are identical. In both cases, the stress on the boundary of the new surface asymptotically approaches a new equilibrium value.

3.2. Irregular Sequence

[25] The same concept that was used to describe flow over a single change in roughness can be applied repeatedly to describe the flow over a boundary having multiple changes in roughness. At the beginning of each distinct set of roughness elements, a new disturbance layer is produced and grows in proportion to the roughness height for that section according to (3). As before, the velocity beneath each disturbance layer can be described by a logarithmic profile. Moving downstream, the disturbance layers stack on top of each other to form a composite outer flow region that scales the wakes of the elements on the boundary. The idea can be further extended to describe the flow over a completely irregular sequence of elements. In this framework, every element is the first bump in a change in roughness problem, and each produces a disturbance

Table 4. Geometry of the Modeled Element Types

Type	H , m	σ , m	σ/H	λ , m	C_D	$\frac{H}{\lambda}C_D$	z_{oTreg} , m
1	0.63	0.85	1.35	3.40	0.63	0.12	0.062
2	0.11	0.14	1.27	0.70	0.67	0.11	0.012
3	0.49	0.29	0.59	1.74	1.13	0.32	0.049
4	0.40	0.41	1.02	2.09	0.81	0.16	0.049

layer that diffuses away from the boundary as shown in Figure 6. Faster growing disturbance layers envelop slower growing layers as is seen in Figure 6. The disturbance layer for each element is distinct from the wake of that element. Turbulent mixing will blur the well-defined boundaries between disturbance layers that are described by this model. Nevertheless, such a model provides a simple way to include the dominant effects of upstream objects on the evolving velocity field.

[26] The sequence of bumps controls the rate at which momentum is lost at the boundary and various sequences produce different average values of the momentum loss (that is, different z_{oT} 's). Drag is a very nonlinear process and the drag on a sequence of bumps divided by the number of bumps can differ substantially from the drag on a bump of average height, average width, and average spacing; therefore the effective z_{oT} 's can vary substantially with streamwise position. A spatially averaged value of z_{oT} over a domain that is determined by the flow depth (better termed a spatially filtered value of z_{oT}) controls the value of the velocity at the surface of a flow no matter what the depth, as long as the depth is finite and no other fluid mechanical effects become important. As depth increases it takes longer for the information on bed or bank roughness to diffuse to the surface and the surface velocity affected by that part of the boundary occurs further downstream. In addition, owing to the diffusive interior of the turbulent flow, the domain over which the boundary roughness is being averaged, namely the effective span of the filter, increases with flow depth.

[27] Provided the effective roughness height of individual elements is known, the height of the disturbance layer can be calculated. The drag on each individual bump is determined in a similar manner that was used to determine the drag on the first bump in the change in uniform roughness problem. In the irregular case, the three regions of the velocity profile used to calculate the reference velocity for each element are the (1) composite outer flow region composed of the logarithmic velocity segments within each disturbance layer, (2) the wake region, and (3) the internal boundary layer region of the upstream element. The same matching conditions are applied between both the wake and the composite outer profile and the wake and the internal boundary layer. The shear velocity for each segment of the outer profile is determined in the same manner as was done for the simple change in roughness problem, by equating the velocities in the upper and lower logarithmic segments at the height of the disturbance layer between the two. From this condition, the shear velocity for the i th disturbance layer above the j th element may be written as

$$\frac{u_{*i}(x_j)}{u_{*i-1}(x_j)} = 1 - \frac{\ln\left(\frac{z_{oi}}{z_{oi-1}}\right)}{\ln\left(\frac{\delta_{DL}(x_j - x_i)}{z_{oi}}\right)} \quad (6)$$

where x_i refers to streamwise distance from an arbitrary upstream datum to the origin of the i th disturbance layer, and x_j refers to distance from this same datum to the center of the j th element.

[28] The roughness height for the set of five small elements (z_{o2}) shown in Figure 6 can be determined using the model for a regular sequence described by *Kean and Smith* [2006]. The same method is used to estimate the roughness heights for individual elements (z_{o1} , z_{o3} , z_{o4}) by assuming their roughness height is approximately the same as it would be for a regular sequence of those elements. This approximation should not lead to significant errors in the predicted height of the disturbance layers, because the height of the layer is a weak function of roughness height ($\sim z_o^{1/5}$), as is seen by *Elliot's* [1958] explicit expression for the height of an atmospheric internal boundary layer:

$$\frac{\delta_{DL}}{z_o} \cong a_o \left(\frac{x}{z_o}\right)^{4/5} \quad (7)$$

where a_o is a constant. In addition, because there is very little curvature to the velocity profile in the outer flow region, the velocity matching conditions between layers will not be seriously affected by errors in the disturbance layer height due to the estimate of z_o .

3.3. Finite Depth

[29] In a finite depth, steady flow over an irregular sequence of elements, the accelerations and decelerations produced by the varying elements can result in changes in the free surface elevation that affect the boundary shear stress. These velocity changes are associated with both an approximately inviscid flow response to the shape of the object, and a resistance response due to the drag on the objects. The change in the free surface elevation due to the approximately inviscid response of the flow is very small if the Froude number is low, and the protrusion height of the bed or bank elements is considerably less than the depth or width of the flow. These conditions are imposed on the remaining calculations of this paper, and are frequently met in natural rivers. The effects of the inviscid flow on the surface elevation could be incorporated iteratively into this model using Bernoulli's equation. The free surface elevation also will be nearly constant if the size of the elements varies about a mean, such that there is not a systematic trend in the average resistance of the elements. Given this constraint, the condition of steady flow can be met by requiring that the integral of the composite outer profile from the boundary to the surface equals the discharge per unit width.

4. Application of the Model

[30] Having developed a method to calculate the flow and boundary shear over an irregular series of roughness elements, we can now address the importance the relative order has on the average boundary shear stress. As an example, this is done by comparing the flow over different configurations of a set of four types of elements. The four types of elements are modeled after the Rio Puerco measurements of bank topography shown in Figure 1 and have the geometry characteristics listed in Table 4. Table 4 also lists the total roughness height for a regular sequence of each element (z_{oTreg}). The low, broad bump of the measured set has been

Table 5. Upstream Flow Properties of the Modeled Channel

Property	Value
Depth	2.5 m
Unit discharge	3.75 m ² /s
Surface velocity	2.0 m/s
τ_T	43.1 N/m ²
z_{oSF}	0.0001 m
z_{oT}	0.049 m
Slope	0.0018

replaced by a sequence of five bumps with geometry similar to that determined from the Fourier analysis of the small-scale features (see Figure 6). A smaller height is used for these five bumps in order to have a greater range in element sizes in the analysis. The four types of elements are embedded within a regular sequence of similar sized elements on the bed of a hypothetical channel having frictionless banks and the geometry and upstream flow properties listed in Table 5. The geometry of the regular elements is the same as type 4 in Table 4. The model also could be applied to the same elements on a channel bank.

[31] Calculations of the average total boundary shear stress on individual elements were made for all 24 possible

configurations of the four element types. Figure 7 shows the calculations for four of these configurations. The results are presented for individual elements as well as for the average of the configuration, and hence highlight both the individual and collective effects of the elements. The four configurations depicted are the measured order 1-2-3-4 (Figure 7a), the reverse of the measured order 4-3-2-1 (Figure 7b), and the bounding configurations, 1-4-2-3 and 3-1-4-2, that produce the highest (Figure 7c) and lowest (Figure 7d) average stress. For reference, the average boundary shear stress of the upstream and downstream series also is shown. In all cases, the drag stress on the elements accounts for over 90% of the total boundary shear stress in each cell, which means that the skin friction available to transport sediment is only 10% of the total stress. Figure 8 shows the calculated velocity profile at the position of the first element of the regular downstream sequence. These results show the logarithmic segments of the disturbance layers that form the composite outer profile, as well as, the wake profile created by the upstream element, which is different in each case.

[32] The calculations of boundary shear stress demonstrate that the drag and resulting stress on an individual

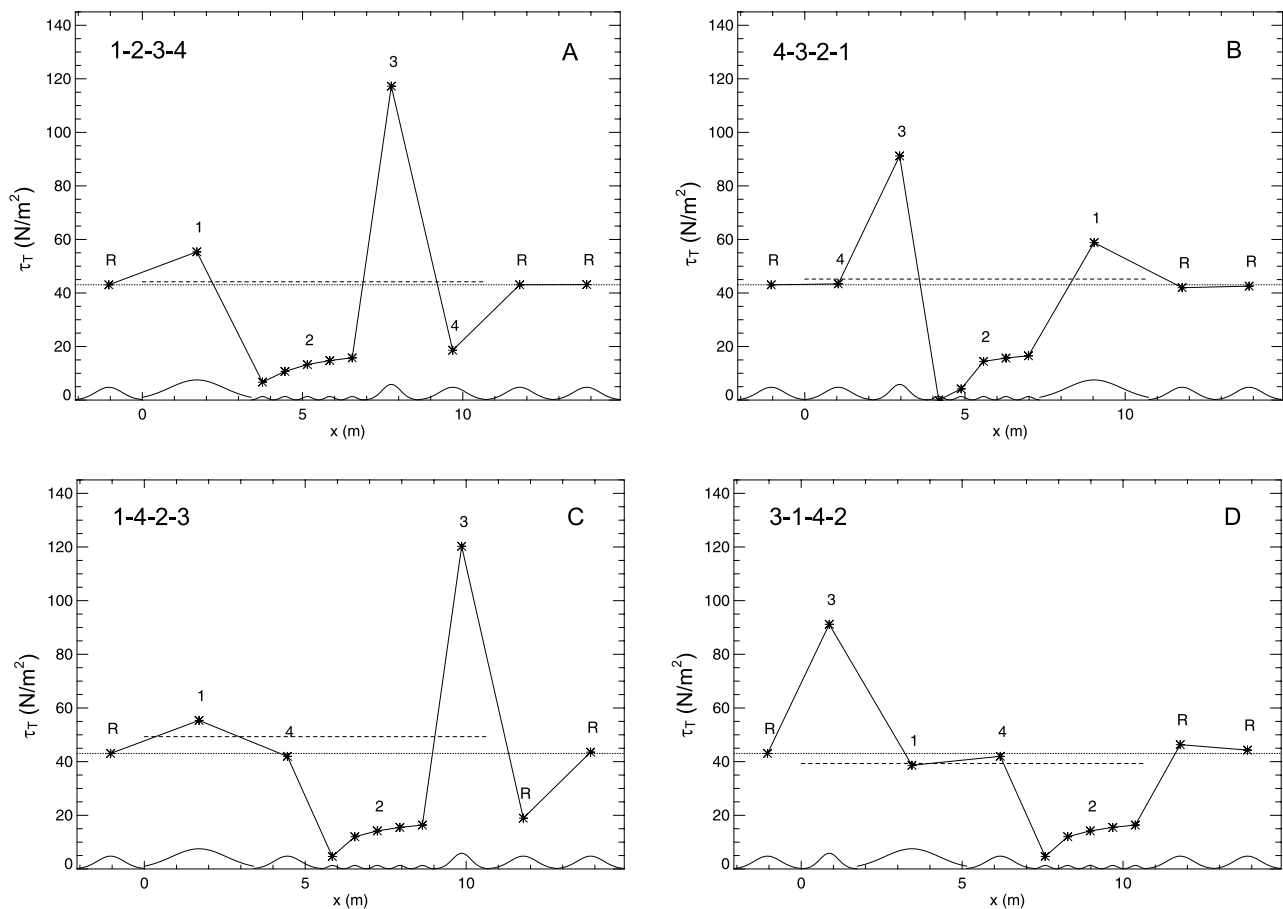


Figure 7. Model calculations of total boundary shear stress (N/m²) averaged over individual elements (symbols) and the set of variable elements (dashed line) for four different configurations, which are (a) 1-2-3-4, (b) 4-3-2-1, (c) 1-4-2-3, and (d) 3-1-4-2. The configuration of the elements is drawn in the background, and the calculated values for each element are labeled by element type. The label “R” denotes the elements that are part of the upstream and downstream regular sequence. The geometry of the regular elements corresponds to type 4. The average upstream boundary shear stress is shown with the dotted line. The flow direction is from left to right.

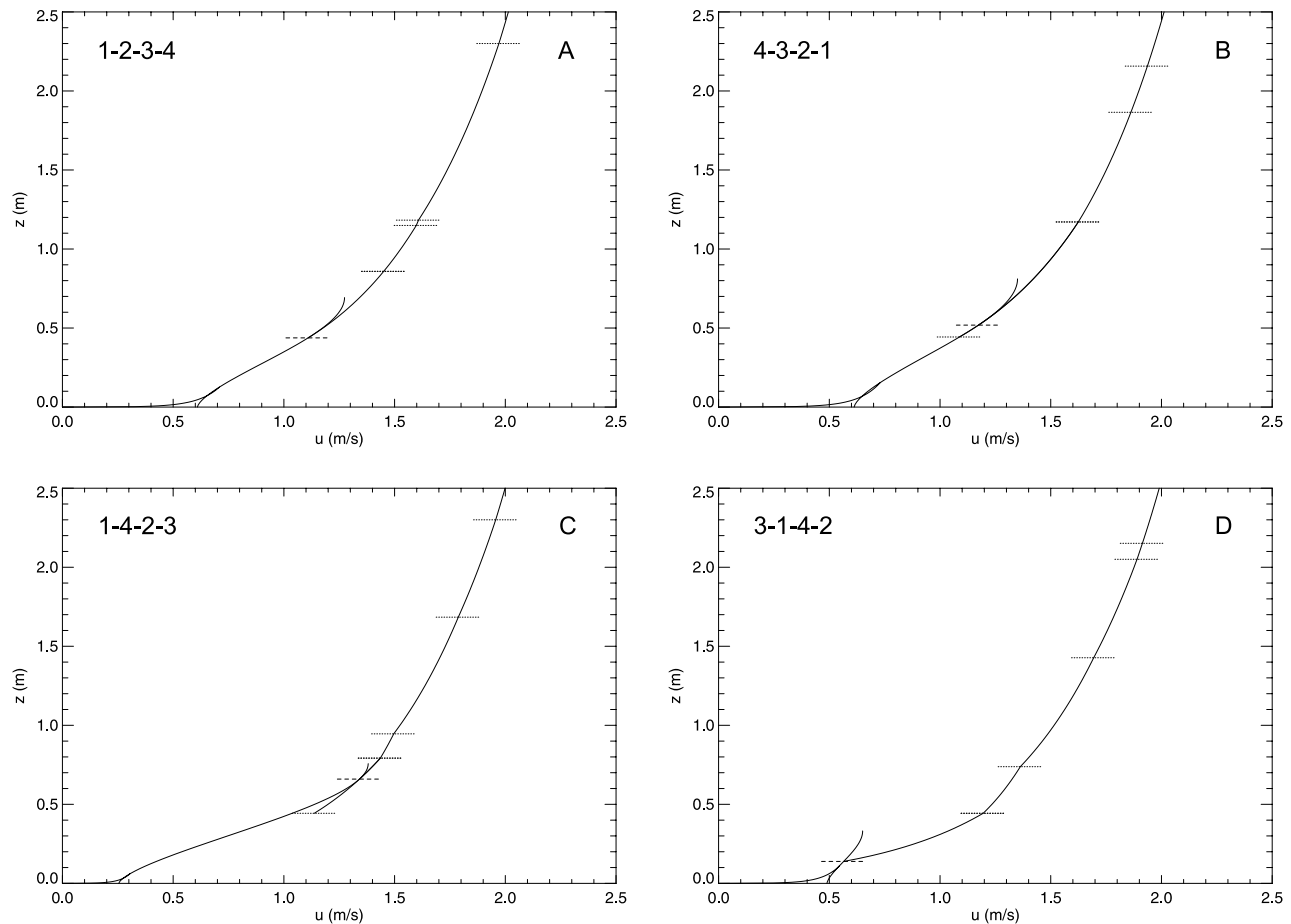


Figure 8. Model calculations of velocity at $x = 11.8$ m, which is the center of the first element of the regular downstream sequence. The lower portion of the profile shows the wake and internal boundary layer that would be in that position if the element were removed from the flow. The dotted lines denote the height of the disturbance layers that form the composite outer profile, and the dashed line denotes the matching height between the wake and this profile. The entire wake profile has been drawn to show the top of the wake.

element is largely dependent on its position in the sequence. This dependence is primarily controlled by the size and shape of the next element upstream. For example, the drag on each element type immediately downstream from the steepest element (type 3) is noticeably lower than its value when a smaller or broader element type is in the upstream position. This result is because these elements are located within the low-velocity zone created by the wake of the steep element. In the extreme case, as seen in Figure 7b, there is almost no drag on the smallest element (type 2) downstream from the steep element, because most of it is within the upstream separation zone. The effect of the largest element (type 1) on elements downstream is not nearly as pronounced as for the steepest element. Although it is taller, its greater breadth gives it a lower drag coefficient and puts more distance between it and the next element downstream. These factors combine to produce a smaller velocity deficit in the wake at the position of the downstream element and, consequently, allow for more drag on it. When elements are located immediately downstream from the sequence of small type 2 elements, the stress and drag on them is higher. The taller elements extend above the wake of the small upstream elements and further into the

faster outer flow, which also has slightly accelerated because of the diminished resistance provided by the small bumps.

[33] The calculations for the configurations that produce the highest and lowest average shear stress for the set (Figures 7c and 7d) further demonstrate the effect of sequence. The lowest stress configuration (3-1-4-2) is one that minimizes the drag on each of the element types. In this configuration, the three largest drag producing elements (3, 1, and 4) are grouped together in such a way that they shelter each other in wakes with large velocity deficits, and hence experience less drag. Moving the steepest bump to the rear of that sequence produces the combination with the highest average shear stress (1-4-2-3). In this configuration, drag on all the elements is maximized, because the two largest drag producing elements, 1 and 3, are separated by the smaller elements, and hence are not sheltered in wakes with large velocity deficits.

[34] The most notable feature of these calculations is that, although the stress on an individual element varies considerably with position, there is relatively little variability in the average stress over the set. The statistics of this stress for the 24 configurations are given in Table 6. The standard

Table 6. Statistics of the Average Boundary Shear Stress on the Set of Four Element Types for All 24 Possible Configurations

	Value
Mean	43.5 N/m ²
Standard deviation	2.9
Maximum (Figure 7c)	49.3 N/m ²
Minimum (Figure 7d)	39.3 N/m ²

deviation of the cases is about 7% of the mean. The mean value of boundary shear stress for all of the configurations also happens to be very close to the value of the upstream shear stress. The good agreement is due to a fortuitous choice for the geometry of the regular sequence and would not be as good had a regular sequence with a substantially higher or lower roughness been chosen.

[35] One reason for the low variability in average stress is because the upstream elements only affect the drag on other elements located a short distance downstream. This can most easily be seen by examining the second regular bump of the downstream sequence ($x = 14$ m) in Figure 7. For all four cases shown, the value of the average boundary shear stress on this bump is nearly the same value regardless of the element type two positions upstream, which is different for each case shown. Although, each of the element types in that position produces a different wake and roughness disturbance, they only substantially affect the drag on the element immediately downstream. Their effect on the second bump downstream is minor.

[36] In order for the stress on the second regular bump to be unaffected by the upstream sequence, the velocity that scales the wake over this element must be nearly the same in all cases. This is already the case a short distance upstream, as can be seen from close inspection of four velocity profiles over the first regular bump near the elevation $z = 0.7$ m (Figure 8). The velocity is the same at this level despite the fact that the profiles are made up of logarithmic segments from different disturbance layers, which are slightly accelerating or decelerating relative to one another, as can be seen by the minor kinks in the profile. The main reason the velocity is the same in all four cases is that each of the profiles must adjust to convey the same discharge. In addition, because all four disturbance layers are present at this position, the small accelerations and decelerations within each of the disturbance layers result in the same velocity near bottom of the profile.

5. Characteristic Geometry of an Irregular Sequence of Topographic Features

[37] The same spatially averaged velocity profile produced by flow over an irregular boundary also can be produced by flow over an equivalently rough boundary composed of identical roughness elements. Simplifying an irregular boundary into an equivalent regular one is particularly useful in modeling more complicated flow situations that can occur near the banks of channels with small-scale

roughness features. Unfortunately, it is not generally possible to specify the geometry of an equivalent regular sequence directly from the measurements of an irregular surface. This difficulty is due in part to the fact that the geometry of the equivalent series is not unique; i.e., there are multiple combinations of H , σ , and λ that define equally rough surfaces composed of identical Gaussian elements. Despite the fact that a general formula for the characteristic geometry of an equivalent sequence is not available, the moments of the statistical distributions of H , σ , and λ can be used to approximate the characteristic geometry for a wide range of irregular surfaces. This approximation is similar to empirical relations for gravel bed roughness, which relate the bed roughness height to the moments of the grain size distribution (e.g., $z_o = 0.1 D_{84}$, where D_{84} is the 84th percentile of the size distribution of the nominal diameter [Whiting and Dietrich, 1989]).

[38] The relation between the moments of the H , σ , and λ distributions and the characteristic regular geometry is determined empirically by applying both the irregular and regular versions of the form drag model. First, the spatially averaged velocity profiles over different irregular sequences of topographic elements are determined using the irregular form drag model described above. The statistical moments of the shape parameters for these cases are used to set the geometry of a regular sequence. The regular version of the form drag model [Kean and Smith, 2006] is then used to compute the spatially averaged velocity profiles over the regular surfaces and the results are compared to the results for the irregular surfaces. A trial and error procedure has been used to identify which moments of the H , σ , and λ distributions define a regular geometry that has equivalent roughness characteristics as the majority of the irregular surfaces.

[39] Ten simulated irregular sequences of topographic features and three field-measured sequences (shown in Figure 3) are used in the analysis. The simulated surfaces consist of a series of 1000 Gaussian-shaped topographic elements. A sample of one of these sequences is shown in Figure 9. The size and shape of each element is chosen at random from lognormal distributions of H and σ/H . This sampling retains the weak correlation between σ and H ($corr \cong 0.65$), which is observed in the measured sequences. Samples outside of three standard deviations from the mean were excluded. The value of λ for each element in the simulated sequence is set to be 4.9σ , which is typical of the measured bank features shown in Figure 3. The means (μ) and standard deviations (ν) defining the lognormal H and σ/H distributions of each simulated case are varied systematically in order to generate surfaces having a spectrum of different roughnesses. Three values for $\mu_{\sigma/H}$ are used to generate sequences having sharp, intermediate, or broad median shapes, with values of $(\sigma/H)_{50}$ equal to 0.5, 1.0, and 2.0. Similarly, three values for both $\nu_{\sigma/H}$ and ν_H are used to generate sequences having high, normal, and low variability in both σ/H and H . Normal variability in σ/H and



Figure 9. First 10 elements in the simulated sequence of case 2 in Table 7. Figure 9 is drawn without any vertical exaggeration.

Table 7. Lognormal Distribution Parameters and Roughness Height for 10 Random Sequences of 1000 Topographic Elements^a

Case	ν_H	$\mu_{\sigma/H}$	$\nu_{\sigma/H}$	z_{oT} , m
1	0.75	0.69	0.65	0.008
2	0.75	0	0.65	0.025
3	0.75	-0.69	0.65	0.041
4	1	0	0.65	0.053
5	0.75	0	0.90	0.019
6	1	0	0.90	0.033
7	1	0.69	0.65	0.011
8	1	-0.69	0.65	0.083
9	0.5	0	0.65	0.016
10	0.75	0	0.40	0.030

^aAll cases have $\mu_H = 2.3$ ($H_{50} = 10$ cm) and $\lambda/\sigma = 4.9$ for every element in the distribution.

H is defined to be $\nu_{\sigma/H} = 0.65$ and $\nu_H = 0.75$. These two values are similar to the values observed in measured topographic sequences (see Tables 2 and 3). All simulated cases have the same μ_H , which corresponds to $H_{50} = 10$ cm. The values of $\mu_{\sigma/H}$, $\nu_{\sigma/H}$, and ν_H for each of the ten simulated cases are summarized in Table 7.

[40] The results of the empirical analysis are shown in Figure 10. Over the range $0.075 < z_{oT}/H_{50} < 0.40$, the characteristic geometry of an irregular sequence is well approximated by

$$\begin{aligned} H_{reg} &= \exp(\mu_H + 1.2\nu_H) = H_{88} \\ \sigma_{reg} &= \exp(\mu_{\sigma} + 1.2\nu_{\sigma}) = \sigma_{88} \\ \lambda_{reg} &= 6H_{88} \end{aligned} \quad (8)$$

where H_{reg} , σ_{reg} , and λ_{reg} are the shape parameters for equivalent regular sequence, and H_{88} and σ_{88} are the 88th percentiles of the H and σ size distributions for the irregular sequence. The spatially averaged flow over surfaces with roughness properties outside this range, such as the Whitewater River and case 8, need to be calculated using the irregular model.

[41] The trends in z_{oT} for the simulated sequences shown in Figure 9 and listed in Table 7 also identify the effects that specific aspects of topographic variability have on flow resistance. The effects of median shape on roughness can be seen by comparing cases 1, 2, and 3. Not surprisingly, surfaces with steeper median shapes are rougher than surfaces with broader median shapes. The effects of variability in size can be seen by comparing cases 2, 4, and 9, which have the same shape characteristics and median height, but different degrees of variability in H . This comparison shows that surfaces having a greater range in H (high ν_H) are rougher (higher z_{oT}) than surfaces having a narrow range of heights. The reason for this trend is that surface roughness is controlled primarily by the larger elements. As ν_H increases from 0.5 to 0.75 to 1.0 in cases 9, 2, and 4, respectively; the size of the larger elements, as measured by H_{88} , increases correspondingly from 18 to 25 to 33 cm. The effects of variability in shape, which are less intuitive, can be seen by comparing cases 2, 5, and 10. These cases are generated from distributions having the same $\mu_{\sigma/H}$ and ν_H , but different values of $\nu_{\sigma/H}$. This comparison shows that surfaces with a greater range of shapes tend to be less rough than surfaces with less variability in shape. One reason for this trend is tied to the relation between C_D of an individual element and shape.

On the basis of the laboratory measurements of *Hopson* [1999], the drag coefficient is modeled to decrease exponentially as shape broadens (see equation (1)). For the comparison between cases 2, 5, and 10, the nonlinear trend in C_D means that the average of the individual drag coefficients for a series of Gaussian elements with high variability in shape will be lower than the average of the individual drag coefficients for a series with less variability in shape. Specifically, as $\nu_{\sigma/H}$ decreases from 0.90 to 0.65 to 0.40 in cases 5, 2, and 10, respectively, the average of the individual drag coefficients for elements greater than or equal to H_{88} in each series increases correspondingly from 0.75 to 0.76 to 0.79. While other nonlinear effects are at work, the trend in the average drag coefficients contributes to making the surfaces progressively rougher.

6. Field Applications

[42] The methods described in this paper for calculating the form drag on small-scale topographic features were developed originally to help (1) address problems of bank erosion and (2) quantify channel flow resistance for the purposes of determining accurate theoretical stage-discharge relations (rating curves). To date, testing the accuracy of these methods has been carried out in the context of the latter objective. These tests, which are described by *Kean and Smith* [2005], were made at two USGS streamflow gauging stations mentioned earlier in this paper (Rock Creek and Whitewater River). The two channels are relatively narrow and, consequently, the bank roughness is an

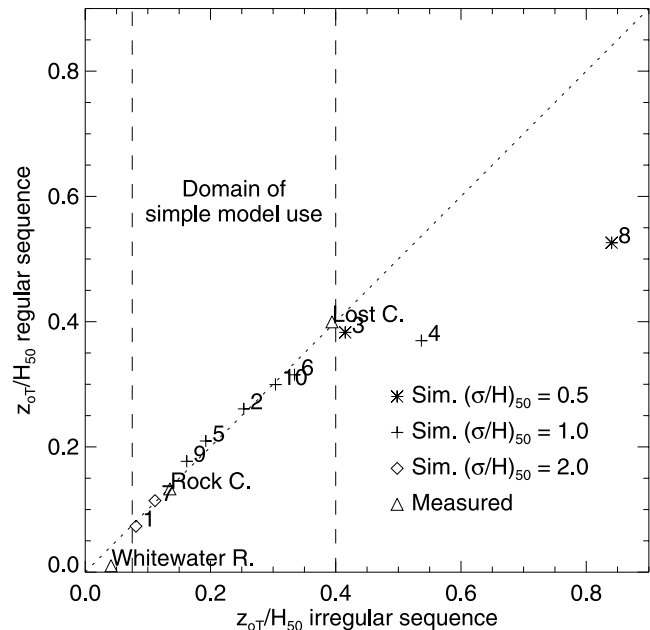


Figure 10. Comparison of the spatially averaged total roughness height for irregular sequences of topographic elements calculated using (1) the model for irregular sequences of elements and (2) the model for regular sequences of identical roughness elements with geometry specified from equation (8). The dashed lines indicate the domain where equation (8) applies. Both measured and simulated sequences are shown. The dotted line is the line of perfect agreement.

important contribution to overall flow resistance in these channels. The form drag model described in this paper was applied to field measurements of bank topography, which are shown in Figure 3 (see also Figure 1 of *Kean and Smith* [2006]). A representative roughness height, z_{oT} , for the banks was determined by the model based on multiple samples of bank topography that were made at different elevations above the bed and at different positions along the reach. Additional field measurements were made to determine the roughness height of the bed and the size and spacing of bank and floodplain vegetation. Those parameters along with the roughness height of the bank and a topographic survey of the reach were used by a specially designed channel flow model to calculate a theoretical rating curve. Other than specifying the bed roughness height using a single low flow discharge measurement, no empirical adjustments were made in the calculation. The calculated theoretical rating curves for the two sites were shown to be in good agreement with discharge measurements made at the sites [*Kean and Smith*, 2005]. While such comparisons, which are designed to assess the overall ability to quantify channel flow resistance as a function of stage, only indirectly test the roughness algorithms outlined in this paper, they nonetheless demonstrate that the method is sufficiently accurate for the purposes of determining discharge in narrow channels. Although the contribution of bank roughness to the total flow resistance of channels with width-to-depth ratios greater than 10 can be very small, bank roughness affects the near-bank flow regardless of the width-to-depth ratio. Given the importance of the near-bank flow in controlling lateral erosion, additional field testing of the methods described in this paper needs to be conducted.

[43] Two additional comments should be made regarding the field application of this model. First, it needs to be emphasized that one of the goals of this work has been to develop a relatively simple tool that can convert basic measurements of complex topography into estimates of surface roughness. For this reason, this work has focused on capturing the essential physics of the problem and has not attempted to address the higher-order effects that are present in flows over complex topography. Second, when modeling flow and sediment transport in rivers a hydrostatic base model usually is employed for computational efficiency. Implicit in taking such an approach is the expectation that all abrupt topographic features, which inevitably produce non hydrostatic pressure fields, are treated as roughness elements. For this reason proper fluid mechanical treatment of such topographic features in a predictive manner is an essential part of modeling flow, sediment transport, and geomorphic adjustment in streams and rivers. Moreover, the ability to separate the effects of form drag from the stress on the actual boundary is required for calculating accurate sediment transport fields and patterns of erosion and deposition in river mechanics and river restoration problems.

7. Summary and Conclusions

[44] This paper presents a method to characterize the roughness properties of irregular fluvial surfaces characteristic of the banks of natural streams and rivers. Field

measurements of bank topography show that (1) the shape of topographic bank features is well approximated by a Gaussian curve, which is specified in terms of three parameters, H , σ , and λ ; and (2) the statistical distributions of these parameters along a bank are approximately lognormal. A model for calculating the flow and boundary shear stress over irregular boundaries composed of Gaussian-shaped topographic elements was developed by generalizing the method of *Kean and Smith* [this issue]. This generalization was accomplished by diffusing the resistance effects of the various features away from the boundary to form an evolving outer profile that scales the wakes of each feature. The model was then used to determine the relative importance of size, shape, and sequence of the topographic features. Model calculations show that drag on an individual topographic feature is primarily controlled by the size and shape of the element immediately upstream. The model also shows that for a given set of different sized elements, the spatial average of the boundary shear stress is only weakly dependent on the sequence of the elements. Finally, the last section of this paper shows that the roughness characteristics of a wide range of irregular sequences of Gaussian-shaped topographic elements can be well approximated by a regular sequence of identical elements having a Gaussian shape defined by H_{88} , σ_{88} , and $\lambda = 6H_{88}$. These relations makes it possible to use the simpler model described in the companion paper [*Kean and Smith*, 2006] to characterize the roughness and flow field over irregular surfaces. A notable direction for future work involves extending the approach to address the flow effects associated with drag on three-dimensional topographic features.

[45] By extending the method described by *Kean and Smith* [2006] to quantify the form drag and roughness of irregular natural sequences of bank topographic features, this study provides an essential second step toward the ability to determine the near-bank flow and boundary shear stress fields that control lateral erosion, as well as make accurate predictions of stage discharge relations.

[46] **Acknowledgments.** Peter Furey and Ricardo Mantilla helped make the multiple bank roughness measurements at Rock Creek. Ned Andrews, Scott Peckham, Jim Pizzuto, and an anonymous reviewer made many helpful suggestions.

References

- Elliot, W. P. (1958), The growth of the atmospheric internal boundary layer, *Eos Trans. AGU*, 38, 1048.
- Friedman, J. M., K. R. Vincent, and P. B. Shafroth (2005), Dating floodplain sediments using tree-ring response to burial, *Earth Surf. Processes Landforms*, 30(9), 1077–1091, doi:10.1002/esp.1263.
- Griffin, E. R., J. W. Kean, K. R. Vincent, J. D. Smith, and J. M. Friedman (2005), Modeling effects of bank friction and woody bank vegetation on channel flow and boundary shear stress in the Rio Puerco, New Mexico, *J. Geophys. Res.*, 110, F04023, doi:10.1029/2005JF000322.
- Hopson, T. M. (1999), The form drag of large natural vegetation along the banks of open channels, M.S. thesis, 114 pp., Univ. of Colo., Boulder.
- Kaimal, J. C., and J. J. Finnigan (1994), *Atmospheric Boundary Layer Flows: Their Structure and Measurement*, 289 pp., Oxford Univ. Press, New York.
- Kean, J. W., and J. D. Smith (2004), Flow and boundary shear stress in channels with woody bank vegetation, in *Riparian Vegetation and Fluvial Geomorphology, Water Sci. Appl. Ser.*, vol. 8, edited by S. J. Bennett and A. Simon, pp. 237–252, AGU, Washington, D. C.
- Kean, J. W., and J. D. Smith (2005), Generation and verification of theoretical rating curves in the Whitewater River Basin, KS, *J. Geophys. Res.*, 110, F04012, doi:10.1029/2004JF000250.

- Kean, J. W., and J. D. Smith (2006), Form drag in rivers due to small-scale natural topographic features: 1. Regular sequences, *J. Geophys. Res.*, *111*, F04009, doi:10.1029/2006JF000467.
- Long, C. E., P. L. Wiberg, and A. R. M. Nowell (1993), Evaluation of von Karman's constant from integral flow parameters, *J. Hydraul. Eng.*, *119*, 1182–1190.
- Miyake, M. (1965), Transformation of the atmospheric boundary layer over inhomogeneous surfaces, M.S. thesis, Dep. of Atmos. Sci, Univ. of Wash, Seattle.
- Schlichting, H (1979), *Boundary-Layer Theory*, 817 pp., McGraw-Hill, New York.
- Smith, J. D., and S. R. McLean (1977), Spatially averaged flow over a wavy surface, *J. Geophys. Res.*, *82*, 1735–1746.
- Walmsley, J. L. (1989), Internal boundary-layer height formulae—A comparison with atmospheric data, *Boundary Layer Meteorol.*, *47*, 251–262.
- Whiting, P. J., and W. E. Dietrich (1989), The roughness of alluvial surfaces: An empirical examination of the influence of size and heterogeneity and natural packing, *Eos Trans. AGU*, *70*(43), 1109.
-
- J. W. Kean and J. D. Smith, U.S. Geological Survey, 3215 Marine Street, E-127, Boulder, CO 80303, USA. (jwkean@usgs.gov)